Atomistic Simulations Of Zr-O-H Systems

B. Szpunar, M.I. Baskes‡, J.A. Szpunar* and P.T. Jochym#
Fuel & Fuel Channel Safety Branch, AECL, Chalk River Laboratories
Chalk River, Ontario, K0J 1J0, Canada
‡ Los Alamos National Laboratory MS G755, Los Alamos, NM 87545, USA
* Department of Metals and Materials Engineering, McGill University,
3610 University St., Montreal, Quebec H3A 2B2, Canada
Institute of Nuclear Physics, ul. Radzikowskiego 152, 31-342 Cracow, Poland

ABSTRACT

The ability of oxygen and hydrogen gas to diffuse through the oxidized Zircaloy sheath on CANDU fuel elements under accident conditions is investigated with a molecular-dynamics approach, employing the Modified Embedded Atom Method (MEAM). Experimental values of the binding energies and the lattice constants, along with the elastic constants of zirconia and zirconium hydride obtained by applying the deformation method based on *ab initio* data (calculated using the Density Functional Theory (DFT)), are used in the parameters of the model development. The calculated energies of vacancies were compared against the predictions by the CASTEP *ab initio* quantum mechanical program, employing density functional theory with Generalized Gradient Approximation. These simulations support previous work which highlights the importance of the effect of cracks and other defects (enhanced diffusion) in modeling oxygen diffusion through fully oxidized Zircaloy sheathing.

INTRODUCTION

This work is an extension of a previous study on model development and simulation of small-scale experiments-performed to improve our understanding of the fundamental processes affecting fission-product release from CANDU fuel elements under accident conditions [1,2].

The initial studies of oxygen and hydrogen diffusion in zirconia were presented in our earlier molecular-dynamics simulations [3] with the use of a rough semi-empirical Modified Embedded Atom Method (MEAM) potential, because of the limited availability of the necessary experimental data used in the fitting parameters of the model. To account for the lack of experimental data, the elastic constants of ZrH_2 and ZrO_2 are calculated using the simple deformational method [4] based on the results of VASP (Vienna *Ab initio* Simulation Package) code *ab initio* calculations [5]. Since knowledge of the mechanical properties of zirconium hydrides is important in the modeling of hydrogen-induced cracking of zirconium, and it is difficult to prepare defect free zirconium hydride samples, present calculations are very useful.

The MEAM is an empirical extension of the embedded atom method (EAM) that includes angular forces [6], and is therefore suitable for studies of nonmetallic systems like oxides. In our later work [2], the improved MEAM potentials for the Zr-H-O system were developed by fitting the elastic properties of zirconia and zirconium hydride in agreement with *ab initio* calculations [2]. In the present work, using these potentials, the energies of vacancies are calculated and compared against the predictions by the CASTEP *ab initio* quantum mechanical program [7], employing density functional theory with Generalized Gradient Approximation [8].

A significant amount of work has been done on molecular dynamics simulations for stabilised zirconia (see e.g. Kilo et al. [9]), but not much on pure zirconia, which will be investigated here.

MODIFIED EMBEDDED ATOM POTENTIALS FOR THE ZR-O-H SYSTEM

The parameters of the improved MEAM potentials for the ternary system Zr-O-H [2] are shown in Table 1. They were derived by slight modification of the parameters for the individual elements which have been developed by Baskes and Johnson [10] for Zr, and by Baskes [6] for O and H.

Table 1: Parameters for the Elements Zr, O and H[a]

Element	E_c	r_e	α	A	$\beta^{(0)}$	$\beta^{(1)}$	$\beta^{(2)}$	$\beta^{(3)}$	$t^{(0)}$	$t^{(1)}$	$t^{(2)}$	$t^{(3)}$	ρ_0
Zr	6.325	3.21	4.46	1.03	3.7	1.0	5.7	1	1	5	4.5	-3.5	0.63
O	2.558	1.21	6.49	1.5	6.49	6.5	6.5	6.5	1	0.09	0.1	0	6.5
H	2.235	0.74	2.96	2.5	2.96	3.0	3.0	3.0	1	0.2	-0.1	0	16

[a] Values listed are the cohesive energy E_c (eV), the equilibrium nearest-neighbor distance r_e (Å), the exponential decay factor α for the universal energy function, the scaling factor A for the embedding energy, the exponential decay factors β for the atomic densities, the weighting factors t for the partial electron densities, and the atomic density scaling ρ_0.

It has been shown [2] that these potentials predict the lattice constants and the cohesive energies of cubic ZrO_2 (Figure 1) and ZrH_2 in good agreement with experimental values. Additionally, in this work the energies of Zr, O, H single-atom vacancies and divacancies of the nearest neighbor atoms: Zr-A (where A indicates an O or H atom) are calculated in ZrO_2 and ZrH_2 respectively (Table 2). The relaxation energy due to atom removal is taken into account, but the binding energies of molecules formed by the removed atoms are not considered. These vacancy energies are compared against the corresponding energies calculated using the CASTEP [7] *ab initio* quantum mechanical program, which employs density functional theory with Generalized Gradient Approximation (Perdew, Wang) [8]. The vacancy energies are calculated by subtracting pseudo-atomic energies from the calculated total energy change due to the removal of an atom. The pseudoatomic energies calculated by CASTEP are respectively: -1277.66 eV for Zr, -430.64 eV for O and -12.45 eV for H atoms. These energies of vacancies calculations were performed to compare the MEAM predictions with CASTEP *ab initio* calculations. Generally they should be bigger than experimentally measured because binding energies of the formed compounds from extracted atoms are not taken into account. All atoms were allowed to relax internally. The respective energies of vacancies for ZrO_2 and ZrH_2 are shown in Table 2. Relaxation affects predominantly the energy of Schottky defects by lowering their energy by 2.36 eV and 0.16 eV for ZrO_2 and ZrH_2 respectively. The calculated energies of vacancies using CASTEP and MEAM agree well with each other (Table 2). The energies of single atom vacancies calculated by MEAM (CASTEP), as presented in Table 2 (24.36 eV (23.68 eV) and 11.33 eV (11.38 eV)), are smaller than those obtained in previous simulations for the energies of defects in ZrO_2 (with an ionic-type of potential) [11], i.e., 86.062 eV for a zirconium vacancy and 14.771 eV for an oxygen vacancy. The corresponding trends, however, are similar.

Table 2: Energy of Zirconium, Oxygen, Hydrogen or ZrA-Type Vacancies[a]

Parameters	ZrO_2		ZrH_2	
	MEAM	CASTEP	MEAM	CASTEP
V_{Zr} (eV)	24.36	23.35	10.57	10.11
V_A (eV)	11.33	11.37	6.04	4.01
V_{ZrA} (eV)[b]	32.49	26.91	15.15	14.51

[a] The calculated values are at 0 K.

[b] V_{ZrA} corresponds to the nearest neighbor atom. An "A"-type atom corresponds to either an oxygen or hydrogen atom in ZrO_2 and ZrH_2.

The energies of the two site defects (32.49 eV and 26.91 eV) are large and may indicate that Schottky defects are created as single site defects that cluster together. The attraction between opposite charge vacancies was reported previously [12]. The previously obtained energies for Schottky trio defects (5.907 eV) [11] and (11.6 eV) [12] are small because the binding energy of the ZrO_2 fragment of extracted atoms is large. The binding energy per ZrO_2 fragment in the bulk (for the experimental lattice constant) can be extracted from the present CASTEP calculations as the difference between the total energy of the fragment in the bulk (-2167.63 eV) and the sum of pseudoatomic energies of the constituent atoms (one Zr atom and two O atoms). The energy obtained in this way (-28.81 eV) is very close to the energy calculated for the equilibrium lattice constant obtained in CASTEP (5.097 Å) for which the total energy per ZrO_2 fragment in the bulk is –2167.64 eV. The energies of a Zr atom vacancy in ZrH_2 calculated by MEAM / CASTEP, as presented in Table 2 (10.57 eV (10.11 eV)), and the energies of a divacancy (ZrH) (15.15 eV (14.51 eV)) are in better agreement with each other than the corresponding energies for hydrogen vacancy (6.04 eV (4.01 eV)).

Elastic Properties

In fitting MEAM parameters, the elastic constants calculated by the *ab initio* method are used [2].

The elastic moduli presented in Table 3 were calculated by applying strain to initially relaxed structures, which for ZrO_2 has been found to be cubic with lattice constants equal to 5.164 and 5.07 Å for VASP and MEAM simulations respectively.

The method used in the elastic constant calculations of ZrH_2 and ZrO_2 by VASP has been described in the earlier work [4]. It is based on results of *ab initio* calculations of the stress tensor of the undeformed and deformed lattices.

For each lattice, a relaxed base structure and several deformed ones were built. The base structure for pure ZrO_2 is cubic with the lattice constant a = 5.164 Å, which is slightly larger than the experimental value for stabilized zirconia (5.07 Å) and the value calculated using the MEAM method (5.07 Å) [2]. In contrast to the MEAM calculations, which predict a cubic structure (δ phase) for ZrH_2, the tetragonal phase (ε) was found in *ab initio* calculations (a = 5.017732 Å, c = 4.447527 Å) in agreement with the experimentally observed structure [13]. This slight distortion is energetically favorable because it splits orbitally degenerate states with a peak in the density of states at the Fermi energy (similarly to that discussed by Switendick for γ phase distortion [14]).

The internal degrees of freedom of deformed unit cells were relaxed and the stresses incurred by the applied strain were calculated. For the ZrO_2 crystal, one tetragonal and one shear deformation were used. For ZrH_2, due to the different symmetry of the unit cell, two types of tetragonal and shear deformations were necessary to obtain a complete set of stresses to build a full equation for all elastic constants of the crystal. In both cases, several magnitudes of the deformation were built, for increased accuracy of the calculation. Shear angles of 0.25º, 0.5º and 1º, and -1%, -0.5%, -0.25%, 0.25%, 0.5% and 1% tetragonal compression/expansion rates were used. The set of linear equations, describing the stress-strain relation for the crystal, built from this data is usually overdetermined and influenced by the inevitable uncertainties in the data. Thus, it is necessary to fit the solution to the set of equations. This is achieved by means of the Singular Value Decomposition algorithm, which is very stable numerically and which automatically provides the least-squares solution [15].

To compare the elastic properties of the tetragonal phase (*ab initio*) with the elastic properties for the cubic phase (MEAM) and the experimentally measured elastic moduli, directional averages are used. The formulas of Reuss [16] and Voigt [17] were employed in these computations, which provide least upper-bound and greatest lower-bound values for the aggregate.

Table 3 shows the calculated results for the bulk (B), shear (G), Young's (Y) modulus and elastic constants at 0 K for ZrO_2 and ZrH_2. The final values of B and G are calculated as an average:

$$B = (B_V + B_R)/2, \quad G = (G_V + G_R)/2 \tag{1}$$

where indexes V and R indicate usage of Reuss or Voigt formulas respectively. The Young's modulus (Y) can be evaluated for an isotropic material as:

$$Y = 9BG/(3B + G) \tag{2}$$

Table 3: Elastic Properties

Property (in GPa)[a]	ZrO_2			ZrH_2		
	Calculated		Experimental	Calculated		Experimental
	VASP	MEAM		VASP	MEAM	
B	235 (230)	218	194 [19]***	133 (130)	134	
G	99	86	95 [19]*** 96-113 [20]*	33	36	
Y	261	228	204.93 [22]** 244-257 [20]*	93	74	82.8 [23]#
B_V	235	218	194 [19]***	133	134	
G_V	113	106	95 [19]*** 96-113 [20]*	35	39	
Y_V	293	274	204.93 [22]** 244-257 [20]*	97	106	82.8 [23]#
B_R	235	218	194 [19]***	133	134	
G_R	85	66	95 [19]*** 96-113 [20]*	32	34	
Y_R	227	179	204.93 [22]** 244-257 [20]*	89	93	82.8 [23]#
c_{11}	489	482	417 [19]*** 400.9 [24] ** 341 [12]*	164	210	
c_{12}	108	86	82 [19]*** 113 [12]*	118	96	
c_{44}	62	45	47[19]*** 103 [12]*	43	26	

a Subscripts V or R indicate that Voight or Reuss formulas were employed in the computations.
* The measurements are for the monoclinic phase.
** Stabilized zirconia
*** Extrapolated to pure zirconia from stabilized zirconia results.
\# The measurements are for 50.6% hydrogen in zirconium hydride.

In the calculation of the elastic moduli within the MEAM method approximation, the internal relaxation of atoms is taken into account, since it is the essential effect in the presence of more than one atom in the primitive unit cell [18]. For the *ab initio* calculations, the bulk modulus was also calculated using an alternative formula (values inside the parentheses):

$$B = -VdP/dV \tag{3}$$

where V is the volume at the pressure P. The elastic constants calculated using VASP and MEAM are in general agreement with each other (better agreement is observed for B and G moduli). They are also in qualitative agreement with the experimental data presented in Table 4. In particular, the c_{11} constant is between 4 and 5 times larger than the c_{12} constant, and the c_{44} constant is about 50% smaller than the c_{12} constant. The elastic moduli (Young's and shear) calculated using Reuss equations lead to lower values than that of Voigt, and their averages (Y, G) agree very well with the limited number of available experimental measurements (Table 4). The low-temperature phase of zirconia is monoclinic, and it is difficult to measure elastic constants at the high temperatures where the cubic phase is stable. Therefore, the results for the elastic constants with derived bulk and shear moduli (values extrapolated from cubic Y_2O_3–doped zirconia data to pure zirconia) [19], as well as the Young's and shear moduli for monoclinic zirconia [20], with the averages over different directions of elastic constants for the monoclinic phase [12] were included. The potential induced breathing (PIB) model, based on the charge density calculated by the linearized augmented plane wave method [21], predicts a bulk modulus equal to 288 GPa and a shear modulus of 189 GPa for cubic zirconia, which is larger than that calculated here by both the *ab intio* and MEAM approximation methods (Table 3). The c_{11} (560 GPa) elastic constant obtained by the PIB [21] method agrees with the value calculated here (489 GPa and 482 GPa), but the c_{44} (180 GPa) and c_{12} (153 GPa) elastic constant values are much larger than the corresponding values in Table 3. In agreement with the experimental measurements and *ab initio* calculations (Table 3), the MEAM approximation predicts c_{12} and c_{44} to be different due to an embedding energy term and angular terms in the potential.

MOLECULAR DYNAMICS SIMULATION

Diffusion in a slab

The MD simulations were performed for a slab of ZrO_2 with 288 atoms (see Figure 2a) and periodic boundary conditions in the z and y directions. The (110) surface has been chosen since it is a more stoichiometric surface than, for example, the (100) surface. The initial relaxations (until 1700 K temperature was reached) were performed for an equivalent bulk structure. Then the surface was created by increasing the periodic length in the x direction. This procedure creates a rough surface due to the relatively large amplitude of vibrations of atoms at 1700 K. The current simulation was performed in order to investigate if the oxidized cladding can act as a physical barrier to either oxygen or hydrogen diffusion at the temperature of the annealing experiment (i.e., 1700 K). The oxygen (Figure 2a) or hydrogen atoms are initially positioned outside the slab at a distance that is shorter than the radius of the cut-off potential. The current simulation (time step equal to 0.0005 ps and 6300 ps simulation time) indicates that while oxygen diffuses into the bulk through the (110) surface (Figure 2b), it does not diffuse through the layer (Figure 2c) but stays close to the surface. The diffusion of other oxygen atoms was investigated and it was found that atoms in the bulk slab do not diffuse, but oxygen atoms on the surface diffuse along the surface layer. In Figure 3, the x (a) and y (b) coordinates (as a function of time) of one of the atoms (which are circled on the left side of Figure 2b) are shown. The x coordinate varies only due to the thermal vibration and the y coordinate changes as the atom migrates along the surface to the position circled on the left side of Figure 2c. The temperature presented in Figure 3c shows oscillations as a function of time but the mean value stays the same and it is equal to 1700 K. Another oxygen atom leaves the same surface of the bulk slab (circled on the left side in Figure 2b) and lands on the other side of the cluster (circled on the right of Figure 2c) due to the periodic boundary condition. The x coordinate of this atom is shown as a function of time in Figure 4a. The (110) surface on the right side of the cluster has more vacancies than the corresponding surface on the left side (Figure 2b). Therefore the x (b) and y (c) coordinates of one of the atoms circled on the right side of Figure 2b are also shown in Figure 4 as a function of time. The atom migrates (Figure 4c-b) from the upper position (Figure 2b) to the lower position on the right side of Figure 2c (not visible).

Hydrogen diffusion on the surface was investigated next by replacing the oxygen atom residing in front of the (110) surface (Figure 2a) with a hydrogen atom. The time step was reduced to 0.00001 ps since the mass of the hydrogen atom is small. It was observed that (at the simulated 1700 K temperature) hydrogen is occasionally kicked out from the surface by thermal excitations and travels through the vacuum to the next available surface due to the periodic boundary condition. Alternatively, it can diffuse along the surface. Eventually, hydrogen becomes trapped (for up to 20 ps) by oxygen atoms at the surface as shown in Figure 5.

Diffusion in bulk

Next, simulations of the diffusion of oxygen and hydrogen atoms in bulk zirconia were performed. Clusters consisting of an ideal structure of zirconia with 324 atoms were created (Figure 6a).

Oxygen diffusion was studied in a cluster without any defects, a cluster with 22 oxygen vacancies (10%), and a cluster with 1 zirconium atom vacancy and 22 oxygen vacancies (created randomly as a single atom vacancy). The current analysis indicates that oxygen does not diffuse in zirconia unless zirconium atom vacancies are present. Even with 10% of oxygen vacancies, no diffusion was observed during a 10 nsec simulation with a time step of 1×10^{-3} psec. In Figures 6b and 6c, the layer with the Zr vacancy (indicated by the empty circle) is shown and the oxygen atom (indicated by arrow) that diffuses (c-new position after 3000 ps) is indicated by the arrow. The variation of the y coordinate (a) of the diffusing oxygen atom is presented in Figure 7a. The temperature, as a function of time, is also shown (Figure 7b) and, as required, represents steady oscillation around 1700 K. The other oxygen atoms (e.g.: indicated by black in Figure 6b), which are not close to the Zr vacancy, do not diffuse during the total simulation time (1.4 ns).

The situation is quite different when a hydrogen atom is embedded in ZrO_2 bulk at 1700 K as shown in Figure 8a. During the simulation time of 2600 ps (Figures 8b and 8c), hydrogen diffuses easily and the variation of x coordinate as a function of time is shown in Figure 9a. The temperature is oscillating around the required temperature 1700 K, as shown in Figure 9b.

Diffusion constant

The calculated diffusion constant for the oxygen atoms on the surface (with the usage of a time step equal to 0.0005 ps and a total time of 6 ns) is equal to 1.8×10^{-11} m^2/s. There are not enough statistics to calculate the diffusion constant of the oxygen atom in the cluster with one Zr vacancy (time step equal to 0.001 ps and total simulation time equal to 14 ns). However, for the cluster with 6 Zr vacancies (maximum time 6 ps) the average (over 3 atoms with the highest diffusion constant) is 13.5×10^{-13} m^2/s (which is comparable to the calculated diffusion constant $9.3\text{x}10^{-13} m^2/s$ for the diffusing oxygen atom shown in Figure 6). These values are much less than the measured experimentally diffusion constant for polycrystalline zirconia ($D = 4.76\times10^{-10}$ m^2/s at 1700 K) [25].

The calculated diffusion coefficient in the bulk is two orders of magnitude smaller than on the surface. The current analysis suggests that for pure zirconia (i.e., without impurities) the experimentally observed oxygen diffusion must take place via defects (e.g., cracks, grain boundaries). Oxygen diffusion has been studied in highly dense nanocrystalline ZrO_2 [26]. It has been found that the diffusion of oxygen at interfaces is three to four orders of magnitude faster than volume diffusion within the entire temperature range studied (450-950°C which corresponds to 720-1220 K). Extrapolated to 1700 K, the diffusion coefficients are 4.15×10^{-14} m^2/s and 5.57×10^{-11} m^2/s for the bulk and interface diffusion of oxygens respectively. The extrapolated diffusion coefficient is lower than reported in Reference [25] since the diffusion coefficient in monoclinic phase is smaller than in the tetragonal phase [25]. These values are in semi-quantitative agreement with current calculations, even though the diffusion was measured for the monoclinic phase.

It has been noticed [26] that diffusivity of oxygen in undoped monoclinic ZrO_2 is, in comparison to the melting temperature, much higher than for other transition metal oxides (e.g., TiO_2, which is chemically very similar, has an extrapolated bulk diffusion of oxygen at 1700 K equal to 9.75×10^{-15} m^2/s). This has been attributed to the instability of the monoclinic phase of zirconia, which at higher temperature transforms to the more dense fluorite structure [26]. The molecular dynamics simulations presented here are unable to reproduce this effect because they predict a stable fluorite structure for all temperatures. The measured activation energy (2.3 eV) for the bulk oxygen diffusion in undoped monoclinic ZrO_2 is nearly twice as high as in Y_2O_3 or CaO stabilized zirconia (0.9-1.3 eV). This is because in doped zirconia the oxygen diffusion is controlled by the migration of structural oxygen vacancies [27]. It has been observed experimentally (in the measurements of oxygen ion conductivity) that the oxygen diffusion coefficient in ytrium stabilised zirconia depends on yttria content and it is the highest for 10 mol % yttria [9,28].

A cluster of 324 atoms (Figure 8a) was created and relaxed at 1700 K to study hydrogen diffusion at constant pressure in defect-free zirconia. The total simulation time was 5000 ps with a time step equal to 0.0001 ps. A hydrogen atom with a zero initial velocity was positioned interstitially (Figure 8a). The analysis indicates that once hydrogen is in bulk zirconia, it can diffuse easily by random jumps (Figure 9a and 9b) and the calculated diffusion constant is 12×10^{-10} m^2/s at 1700 K. This value is one order of magnitude lower than the measured diffusion constant of hydrogen in metallic zirconium extrapolated to 1700 K (29.66×10^{-9} m^2/s [29] and 29.92×10^{-9} m^2/s [30]), but it is much higher than the measured diffusion constants for polycrystalline dense oxides extrapolated to 1700 K (again the monoclinic – cubic phase transition is neglected): ZrO_2 film on Zr (9.328×10^{-15} m^2/s [31]) and ZrO_2 film on Zr-2.5 Nb (6.72×10^{-16} m^2/s [31]). The reason for the difference between the measured diffusion constants in ZrO_2 films on different substrate is not exactly known since there are many effects which may play a role (e.g., residual stresses, dislocation density, segregation). It also varies with temperature. The extrapolated values of the diffusion constants at room temperature (4.1412×10^{-30} m^2/s and 1.3417×10^{-22} m^2/s for layers on pure Zr and Zr-2.5 Nb respectively [31]) differ greatly, because of the factor of 2 difference in the activation energies (100.1 kJ/mol and 53.7 kJ/mol, respectively).

The calculated diffusion constant of hydrogen in zirconia, however, is of the same magnitude as the measured hydrogen diffusion constants (extrapolated to 1700 K) in oxides grown on Zircaloy-2 (81.7×10^{-10} m^2/s) and Zr-15 wt% Nb (35×10^{-10} m^2/s) [32].

There have been other recent studies of hydrogen diffusion in various oxidized zirconium alloys [33]. The diffusivity at room temperature varied between 1.26×10^{-12} m^2/s and 1.51×10^{-12} m^2/s, and decreased as the relative fraction of tetragonal zirconia increased (between 0.9% and 12%). It was also suggested that charged (positive) precipitates created during zirconium oxidation may act as a hydrogen trap and lower diffusivity. The higher diffusion of hydrogen in zirconia alloys was attributed to the diffusion through the interconnected pores and unoxidized regions [31]. Our calculations probably overestimate hydrogen diffusion in zirconia because the potential used currently predicts a lower binding energy between hydrogen and oxygen, but studies of hydrogen dissolution [34] and release in nonmetals (uranium dioxide) show a solubility dependence on the square root of the gas pressure, which indicates hydrogen dissolution in atomic form. Also, the principal form of released hydrogen was H_2 with very little water observed [34]. Extrapolated to 1700 K, the measured value of hydrogen diffusion in urania is 5.3×10^{-8} m^2/s [35], which is two orders of magnitude higher than calculated here for hydrogen diffusion in zirconia.

ELECTRON DENSITY AND HYDROGEN DIFFUSION

It is interesting that hydrogen, which diffuses readily into metals, stays on ZrO_2 surfaces and its diffusion in zirconia is smaller, by orders of magnitude, than that in pure zirconium. The trapping of hydrogen in the presence of oxygen can be understood in terms of the change in electron density as the zirconium is oxidized. The electronic-structure calculations for pure zirconium, ZrO_2 and ZrH_2 were performed (at a temperature of 0 K) using a tight-binding linear muffin-tin orbital atomic-sphere approximation [36]. The cubic unit cell presented in Figure 1 was used in the current calculations. The charge densities are calculated for a (100) plane positioned in the unit cell (Figure 1) at a distance of 0.125 c from the bottom zirconium atoms (i.e., this position is in the middle between a plane containing zirconium and one containing oxygen in the unit cell).

The electron charge densities of zirconium and ZrO_2 are shown in Figures 10a and 10b respectively. It can be seen that the electron densities in metallic zirconium are evenly distributed between 0.02 and 0.05 $bohr^{-3}$, whereas in zirconia the electrons are shifted towards the oxygen atoms with minimum and maximum densities of 0.01 and 0.16 $Bohr^{-3}$ respectively. Interestingly, as shown by Norskov [37], the hydrogen energy is strongly dependent on the electron density within which it is embedded. Thus, it can be seen that hydrogen can become trapped in zirconia at the electron densities where its energy is at a minimum (i.e., when surrounded by a high-energy barrier as created by high electron densities from oxygen). Hence, these electron density calculations further show that hydrogen can be trapped on the surface of zirconia as observed in the current simulations. The charge density of zirconium hydride (Figure 10c) fluctuates between 0.02 and 0.07 $Bohr^{-3}$ (similar to that for pure zirconium) with the extra charge close to the hydrogen atoms.

SUMMARY

The MEAM semi-empirical potentials have been developed for Zr-O-H system. The calculated energies of vacancies and the elastic modules using *ab initio* method and MEAM agree well with each other. The calculated elastic moduli of zirconium hydride may be useful in the analysis of hydrogen-induced cracking of zirconia.

Semi-empirical atomistic simulations and *ab initio* electronic structure calculations indicate that oxygen and hydrogen cannot diffuse effectively through a slab of pure

ZrO_2. To account fully for the observed diffusivity of oxygen in zirconium dioxide, diffusion through cracks or other defects (e.g., grain boundaries) has to be included in the simulation. It is also found that zirconium vacancies are needed for oxygen diffusion to occur in zirconia. By doping zirconia with Y or Ca, a charge imbalance is created, and to fulfill the charge neutrality, oxygen vacancies are created, which will therefore enhance the oxygen diffusion. To study the effect of impurities on the diffusion of oxygen and hydrogen in doped zirconia, combined MEAM and *ab initio* simulations must be considered due to the complexity of interactions between the atoms.

ACKNOWLEDGEMENTS

One of the authors (B. Szpunar) acknowledges support by B.J. Lewis (in the beginning of this work [1,3]) and RMC (especially T. Winsor & M. Watt) for providing free access to computer facilities. The authors would like to thank B.J. Lewis, D. Khatamian, W.H. Hocking, R.S. Dickson, L.W. Dickson, D.B. Sanderson, F.C. Iglesias, D. Than, V. Krstic for many helpful comments, and O. Jepsen and MPI-Stuttgart for providing the TB-LMTO-ASA code. M.I. Baskes acknowledges support from the USDOE. J.A. Szpunar acknowledges NSERC support.

REFERENCES

[1] Szpunar B., Lewis B.J., Arimescu V.I., Dickson R.S., Dickson L.W., "Three-Component Gas Mixture Transport in Defective CANDU Fuel Rods", J. Nucl. Mater. **294**, 315 (2001).

[2] Szpunar B., Baskes M.I., Jochym P.T., "Oxygen and Hydrogen Diffusion in Zirconia", 8th International Conference on CANDU Fuel, 2003 September 21-24, Delawana Inn, Honey Harbour, Ontario, Canada, Conference Proceedings (2003).

[3] Szpunar B., Lewis B.J., Arimescu V.I., Dickson R.S., Dickson L.W. and Baskes M.I., "Three-Component Gas Mixture Transport in Defective CANDU Fuel Rods", 7th International Conference on CANDU Fuel, 2001 September 23-27, Kingston, Ontario, Canada, Conference Proceedings vol. 1, 329 (2001).

[4] Jochym P.T., Parlinski K., "Elastic Properties and Phase Stability of AgBr Under Pressure", Phys. Rev. **B 65**, 24106 (2002).

[5] Kresse G. and Furthmüller J., "Efficient iterative schemes for ab initio total-energy calculations using a plane-wave basis set", Phys. Rev. **B54**, 11169 (1996).

[6] Baskes M.I., "Modified Embedded-Atom Potentials for Cubic Materials and Impurities", Phys. Rev. **B46**, 2727 (1992).

[7] Segall M.D., Lindan P L.D., Probert M.J., Pickard C.J., Hasnip P.J., Clark S.J. and Payne J.D., "First-principles simulation: Ideas, illustrations and the CASTEP code", J. Phys. Cond. Matt. **14**, 2717 (2002).

[8] Perdew, P., Wang Y., "Accurate and simple analytic representation of the electron-gas correlation energy", Phys. Rev. **B45**, 13244 (1992).

[9] Kilo M., Argirusis C., Borchardt G., Jackson R.A., Phys. Chem. Chem. Phys. **5,** 2219 (2003).

[10] Baskes M.I. and Johnson R.A., "Modified Embedded Atom Potentials for HCP Metals", Modelling Simul. Mater. Sci. Eng. **2**, 147 (1994).

[11] Dwivedi A., Cormack A.N., "A Computer Simulation Study of the Defect Structure of Calcia-Stabilized Zirconia", Phil. Mag. **61**, 1 (1990).

[12] Mackrodt W.C. and Woodrow P.M., "Theoretical Estimates of Point Defect Energies in Cubic Zirconia", J. Am. Ceram. Soc. **69**, 277 (1986).

[13] Mueller W.M., Blackledge J.P., Libowitz G.G., *Metal Hydrides* (Academic Press) (1968).

[14] Switendick A.C., "Electronic structure of gamma phase zirconium hydride", J. Less-Common Met. **103**, 309 (1984).

[15] Press W.H., Flamery B.P., Tenkolsky S.A., and Vetterling W.T., *Numerical Recipes* (Cambridge University Press, Cambridge, New York, Melbourne) (1988).

[16] Reuss A., "Berechnung der FlieBgrenze von Mischkristallen auf Grund der Plastizitatsbedingung fur Einkristalle", Z. Angew. Math. Mech. **9**, 49 (1929).

[17] Voigt W., *Lehrbuch der Krystallphysik* (ed. B.G. Teubner, Leipzig) (1928).

[18] Lutsko J.F., "Generalized expressions for the calculation of elastic constants by computer simulation", J. Appl. Phys. **65**, 2991 (1989).

[19] Kandil H.M., Greiner J.D. and Smith J.F., “Single-Crystal Elastic Constants of Yttria-Stabilized Zirconium in the Range 20 to 700ºC”, J. Am. Ceram. Soc. **67**, 341 (1984).

[20] Smith C.F. and Crandall W.B., “Calculated High-Temperature Elastic Constants for Zero Porosity Monoclinic Zirconia”, J. Am. Ceram. Soc. **47**, 624 (1964).

[21] Cohen R.E., Mehl M.J. and Boyer L.L., “Phase Transitions and Elasticity in Zirconia”, Physica **B150**, 1 (1988).

[22] Shackelford J.F., Alexander W. and Park J.S., *Materials Science and Engineering Handbook* (CRC Press, Boca Raton, Ann Arbor, London, Tokyo) (1992).

[23] Parker D.S. and Huffine C.I., “Properties of Hydrided Zirconium”, USAEC, Report APEX-561, General Electric Company (1959).

[24] Nevitt M.V., Chan J.Z., Liu J.Z., Grimisditch M.H. and Fang Y., “The Elastic Properties of Monoclinic ZrO_2”, Physica **B150**, 230 (1988).

[25] Iglesias F.C., Sagat S. and Sills H.E., “High Temperature Oxidation of Zircaloy”, Res. Mechanica **17**, 125 (1986).

[26] Brossman U., Wurschum R., Sodervall U. and Schaefer H.-E., “Oxygen Diffusion in Ultrafine Grained Monoclinic ZrO_2”, J. Appl. Phys. **85**, 7646 (1999).

[27] Alta C.R. and Kwok Chee-Kin, “Fundamental Optical Absorption Edge of Sputter-Deposited Zirconia and Yttria”, J. Am Ceram. Soc. **73**, 3209 (1990).

[28] Kondoh J., Kawashima T., Kikuchi S., Tomi Y. and Ito Y., “Effect of aging on yttria-stabilized zirconia. I. Study of its electrochemical properties”, J. Electrochem. Soc. **145I**, 1527 (1998).

[29] Hashizume K., Sugisaki M., Hatano K., Ohmori T. and Ogi K., “Application of Discharge Implantation Method to Measurement of Diffusion Coefficient of Hydrogen Isotopes in Zirconium”, J. Nuclear Science and Technology, **31**, 1294 (1994).

[30] Kearns J.J., “Diffusion Coefficient of Hydrogen in Alpha Zirconium, Zircaloy-2 and Zircaloy-4”, J. Nucl. Mater. **43**, 330 (1972).

[31] Khatamian D. and Manchester F.D., “An Ion Beam Study of Hydrogen Diffusion in Oxides of Zr and Zr-Nb (2.5 wt%)”, J. Nucl. Mater. **166**, 300 (1989).

[32] Khatamian D., “Hydrogen Diffusion in Oxides Formed on Surfaces of Zirconium Alloys”, J. Alloys and Comp**. 253-254**, 471 (1997).

[33] Byung Hyuck Lim, Hyun Seon Hong and Kyung Sub Lee, “Measurements of hydrogen permeation and absorption in zirconium oxide scales”, J. Nucl. Mater. **312**, 134 (2003).

[34] Sherman D.F. and Olander D.R., “Hydrogen Dissolution in and Release from Nonmetals, I. Uranium Dioxide”, J. Nucl. Mater. **166**, 307 (1989).

[35] Wheeler V.J., “The Diffusion and Solubility of Hydrogen in Uranium Dioxide Single Crystals”, J. Nucl. Mater. **40**, 189 (1971).

[36] Andersen O.K., Jepsen O. and Sob M., *Electronic Band Structure and its Applications* (edited by M. Yussouff, Springer Verlag, Berlin) 1 (1986).

[37] Nørskov J.K., “Chemisorption on Metal Surfaces”, Rep. Prog. Phys. **53**, 1253 (1990).

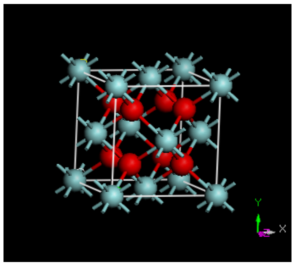

Figure 1
Unit cell of ZrO_2 (blue and red balls are correspondingly zirconium and oxygen atoms respectively).

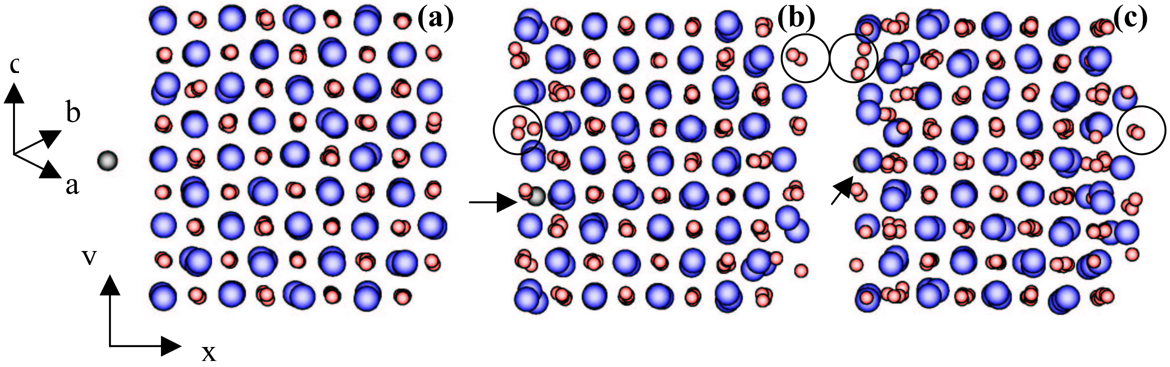

Figure 2
a) Slab (110) (initial configuration) with external oxygen on free surface (black).
b) Slab (110) after 100 ps and 6000 ps (c) with the external oxygen (black) indicated by arrow. Blue and red balls represent zirconium and oxygen atoms

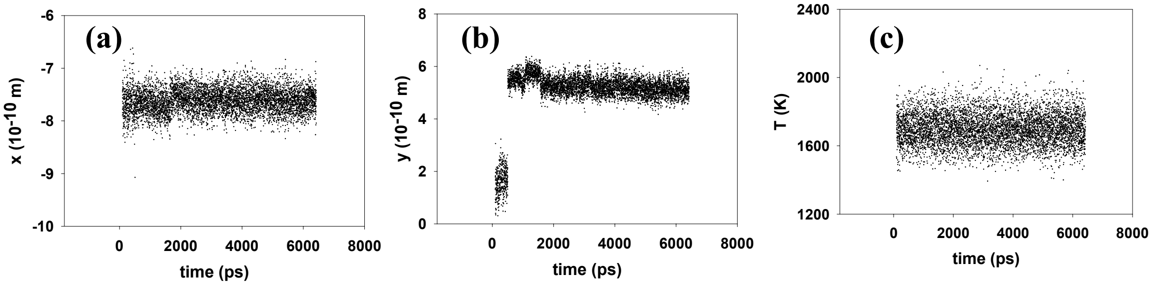

Figure 3
The x (a) and y (b) coordinates (as a function of time) of one of the atoms which are circled on the left side of Figure 2b and which migrates to the position circled on the left of Figure 2c. The temperature is also shown as a function of time (c).

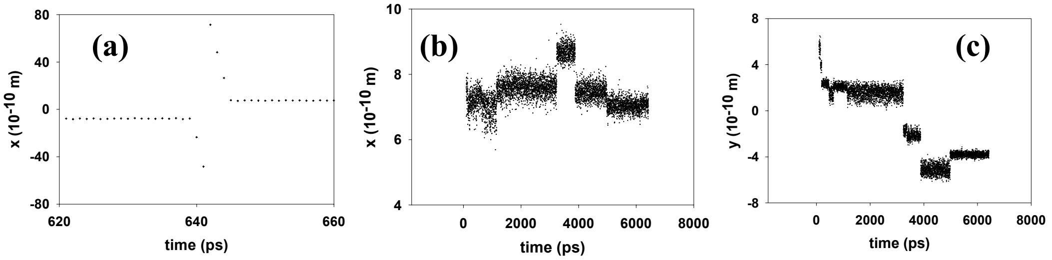

Figure 4
The x coordinate of another atom (circled on the left side of Figure 2b) which is kicked out from the surface and lands on the other side of the cluster (circled on the right of Figure 2c) due to the periodic boundary condition is shown in figure 4a as a function of time. The x (b) and y (c) coordinates (as a function of time) of the atom from the circle on the right of Figure 2b which migrates to the lower position on the right side of Figure 2c (not visible).

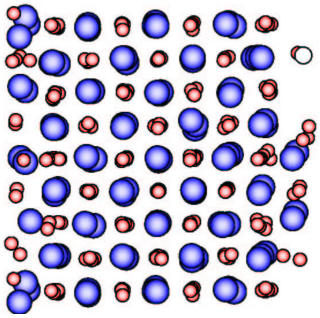

Figure 5
Hydrogen atom (white) on ZrO_2 (110) slab (20 ps).

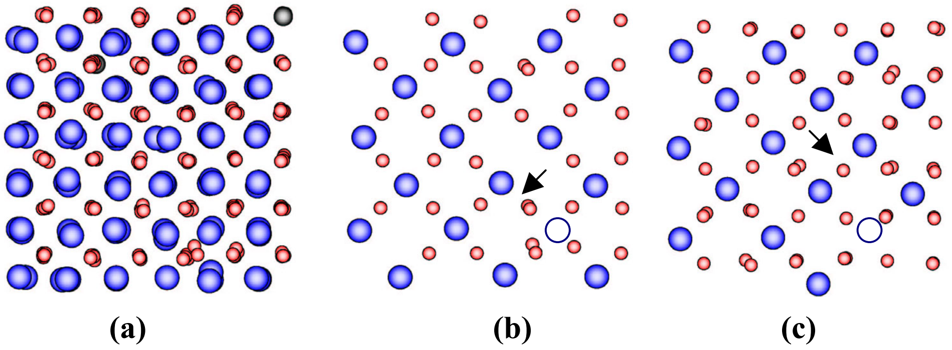

n) with selected oxygen atoms (black) which
(b) Selected layer (initial configuration) with Zr
) and oxygen atom (indicated by arrow) which
diffuses after 1000 ps (c-new position after 3000 ps indicated by arrow).

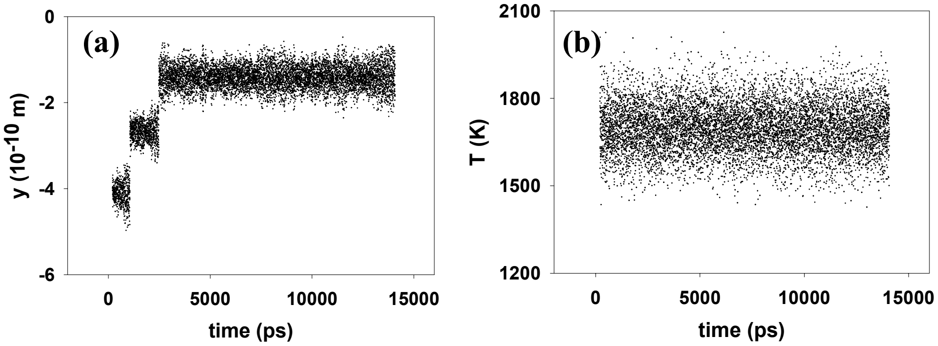

Figure 7
Variation of the y coordinate (a) of the oxygen atom that diffuses in bulk ZrO_2. The temperature is also shown as a function of time (b).

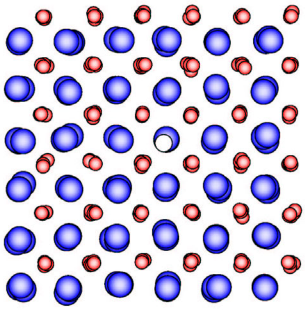

Figure 8a
Hydrogen (indicated as white) in bulk ZrO_2 (initial configuration).

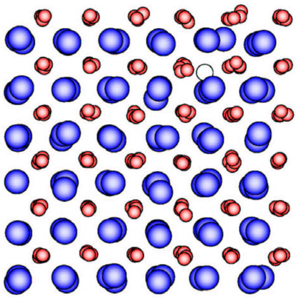

Figure 8b
Hydrogen (50 ps) in bulk ZrO_2.

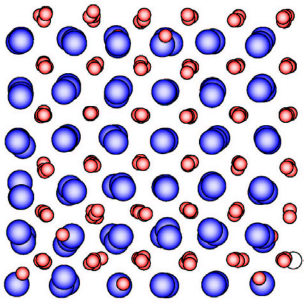

Figure 8c
Hydrogen (2570 ps) in bulk ZrO_2.

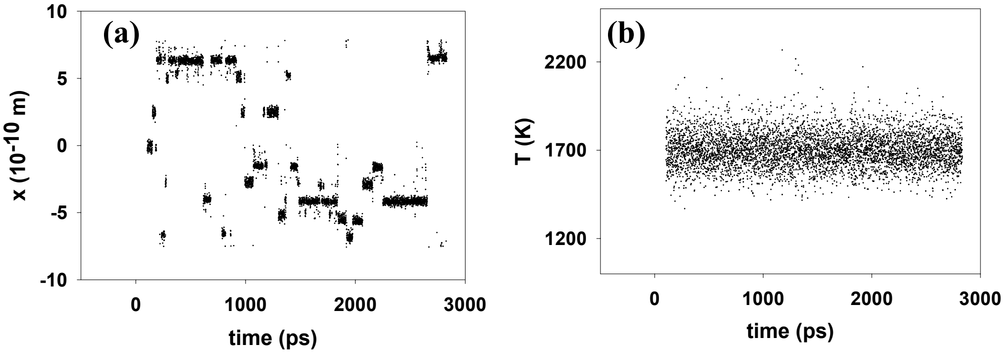

Figure 9
Hydrogen x coordinate (a) and temperature (K) (b) as a function of time.

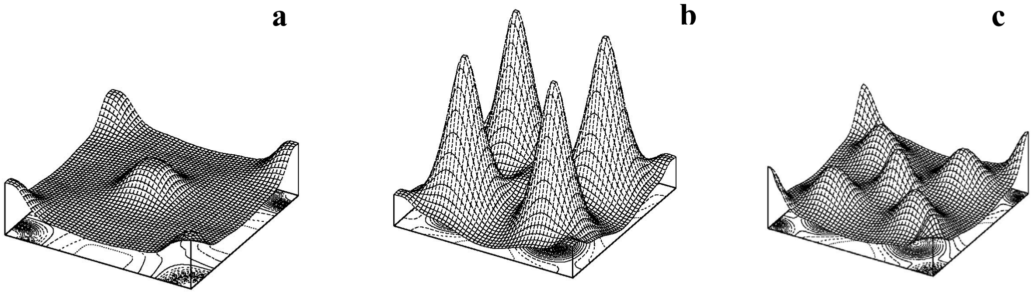

Figure 10
Charge density of zirconium (a), zirconia (b) and zirconium hydride (c).